

BMDS-Net: A Bayesian Multi-Modal Deep Supervision Network for Robust Brain Tumor Segmentation

YAN ZHOU*, School of Mathematics and Statistics, Changsha University of Science and Technology, China

ZHEN HUANG, School of Mathematics and Statistics, Changsha University of Science and Technology, China

YINGQIU LI, School of Mathematics and Statistics, Changsha University of Science and Technology, China

YUE OUYANG, School of Mathematics and Statistics, Changsha University of Science and Technology, China

SUNCHENG XIANG*, School of Biomedical Engineering, Shanghai Jiao Tong University, China

ZEHUA WANG†, Shanghai Chest Hospital, Shanghai Jiao Tong University School of Medicine, China

Accurate brain tumor segmentation from multi-modal magnetic resonance imaging (MRI) is a prerequisite for precise radiotherapy planning and surgical navigation. While recent Transformer-based models such as Swin UNETR have achieved impressive benchmark performance, their clinical utility is often compromised by two critical issues: sensitivity to missing modalities (common in clinical practice) and a lack of confidence calibration. Merely chasing higher Dice scores on idealized data fails to meet the safety requirements of real-world medical deployment. In this work, we propose **BMDS-Net**, a unified framework that prioritizes **clinical robustness and trustworthiness** over simple metric maximization. Our contribution is three-fold. First, we construct a robust deterministic backbone by integrating a **Zero-Init Multimodal Contextual Fusion (MMCF)** module and a **Residual-Gated Deep Decoder Supervision (DDS)** mechanism, enabling stable feature learning and precise boundary delineation with significantly reduced Hausdorff Distance, even under modality corruption. Second, and most importantly, we introduce a **memory-efficient Bayesian fine-tuning strategy** that transforms the network into a probabilistic predictor, providing voxel-wise uncertainty maps to highlight potential errors for clinicians. Third, comprehensive experiments on the BraTS 2021 dataset demonstrate that BMDS-Net not only maintains competitive accuracy but, more importantly, exhibits superior stability in missing-modality scenarios where baseline models fail. The source code is publicly available at <https://github.com/RyanZhou168/BMDS-Net>.

CCS Concepts: • Computing methodologies → Computer vision tasks; • Applied computing → Health informatics.

Additional Key Words and Phrases: Brain tumor segmentation, Multi-modal MRI, Deep supervision, Robustness, Uncertainty estimation

ACM Reference Format:

Yan Zhou, Zhen Huang, Yingqiu Li, Yue Ouyang, Suncheng Xiang, and Zehua Wang. 2026. BMDS-Net: A Bayesian Multi-Modal Deep Supervision Network for Robust Brain Tumor Segmentation. *ACM Trans. Multimedia Comput. Commun. Appl.* 1, 1 (January 2026), 16 pages. <https://doi.org/XXXXXX.XXXXXXX>

*Both authors contributed equally to this research.

†Corresponding author.

Authors' Contact Information: Yan Zhou, yanzhou@stu.csust.edu.cn, School of Mathematics and Statistics, Changsha University of Science and Technology, Changsha, Hunan, China; Zhen Huang, School of Mathematics and Statistics, Changsha University of Science and Technology, Changsha, China; Yingqiu Li, School of Mathematics and Statistics, Changsha University of Science and Technology, Changsha, China; Yue Ouyang, School of Mathematics and Statistics, Changsha University of Science and Technology, Changsha, China; Suncheng Xiang, School of Biomedical Engineering, Shanghai Jiao Tong University, Shanghai, China; Zehua Wang, sjtu_wzh@sjtu.edu.cn, Shanghai Chest Hospital, Shanghai Jiao Tong University School of Medicine, Shanghai, China.

Permission to make digital or hard copies of all or part of this work for personal or classroom use is granted without fee provided that copies are not made or distributed for profit or commercial advantage and that copies bear this notice and the full citation on the first page. Copyrights for components of this work owned by others than the author(s) must be honored. Abstracting with credit is permitted. To copy otherwise, or republish, to post on servers or to redistribute to lists, requires prior specific permission and/or a fee. Request permissions from permissions@acm.org.

© 2026 Copyright held by the owner/author(s). Publication rights licensed to ACM.

Manuscript submitted to ACM

1 Introduction

Accurate brain tumor segmentation from magnetic resonance imaging (MRI) is a cornerstone for diagnosis, radiotherapy planning, and longitudinal assessment of gliomas. In routine clinical workflows, delineating tumor sub-regions is time-consuming and subject to inter-rater variability, motivating reliable automatic segmentation. The *Brain Tumor Segmentation* (BraTS) benchmark has become the de facto evaluation platform for this problem, providing multi-institutional multi-modal MRI data and standardized labels for clinically relevant sub-regions such as Whole Tumor (WT), Tumor Core (TC), and Enhancing Tumor (ET) [2, 3, 16, 20].

Driven by the BraTS benchmark, deep learning approaches for brain tumor segmentation have rapidly evolved over the past decade. Early studies primarily adopted encoder-decoder CNN architectures, such as U-Net and its 3D variants, to capture local spatial patterns in volumetric MRI data [12, 21, 24–26]. Subsequent work focused on improving robustness and generalization through careful pipeline design. Notably, nnU-Net demonstrates that automated configuration of preprocessing, architecture, and training strategies can yield strong and reliable baselines across a wide range of biomedical segmentation tasks [13]. More recently, vision Transformers have been introduced to medical image segmentation to overcome the limited receptive fields of CNNs by leveraging global context modeling via self-attention [5, 30]. Architectures such as UNETR and Swin UNETR show that hierarchical Transformer backbones, including the Swin Transformer, can provide powerful representations for 3D multi-modal brain tumor segmentation [8, 9, 19]. In parallel, alternative sequence modeling and lightweight attention paradigms have recently been explored in medical image segmentation. For instance, MALUNet [29] introduces a lightweight multi-attention mechanism for efficient lesion segmentation, while VM-UNet incorporates Vision Mamba into a U-shaped architecture, demonstrating diverse backbone potential for medical tasks [28].

To systematically analyze the field’s progression, we visualize the landscape of brain tumor segmentation in Figure 1. The field has evolved from **Era 1: CNN Foundations**, characterized by robust but local feature extraction (e.g., nnU-Net), to **Era 2: Transformer Adoption**, which leverages global context to chase state-of-the-art (SOTA) benchmarks. However, as illustrated in the red dashed region of Figure 1, this transition has introduced a paradox: while Era 2 models achieve higher Dice scores, they often become “fragile”—exhibiting extreme sensitivity to missing modalities and lacking uncertainty quantification. Previous attempts to address these reliability issues have been largely **fragmented specialized solutions** (purple region), offering specific fixes such as HeMIS for missing modalities or Deep Ensembles for uncertainty, without a unified architecture. **BMDS-Net** is designed to occupy the “Proposed Frontier” (blue region), bridging the gap between the high accuracy of Transformers and the trustworthiness required for clinical viability.

However, high performance on standardized benchmarks does not always translate to clinical utility. Current research in brain tumor segmentation has largely prioritized marginal improvements in Dice scores under idealized settings, often overlooking the robustness and safety requirements of real-world clinical deployment. In routine practice, MRI acquisitions frequently suffer from missing or corrupted modalities due to patient motion, time constraints, or scanner variability. Standard early-fusion architectures, which implicitly assume all modalities to be equally reliable, can therefore exhibit catastrophic performance degradation when even a single sequence is unavailable, making their predictions unstable and potentially misleading. Beyond robustness, most state-of-the-art segmentation networks remain deterministic black boxes, producing a single segmentation mask without conveying any notion of confidence. In high-stakes applications such as neurosurgical planning and radiotherapy, boundary precision—commonly evaluated by Hausdorff Distance—is critical for preserving functional tissue, and clinicians must be able to identify regions where model predictions are uncertain. Bayesian deep learning provides principled mechanisms for quantifying epistemic

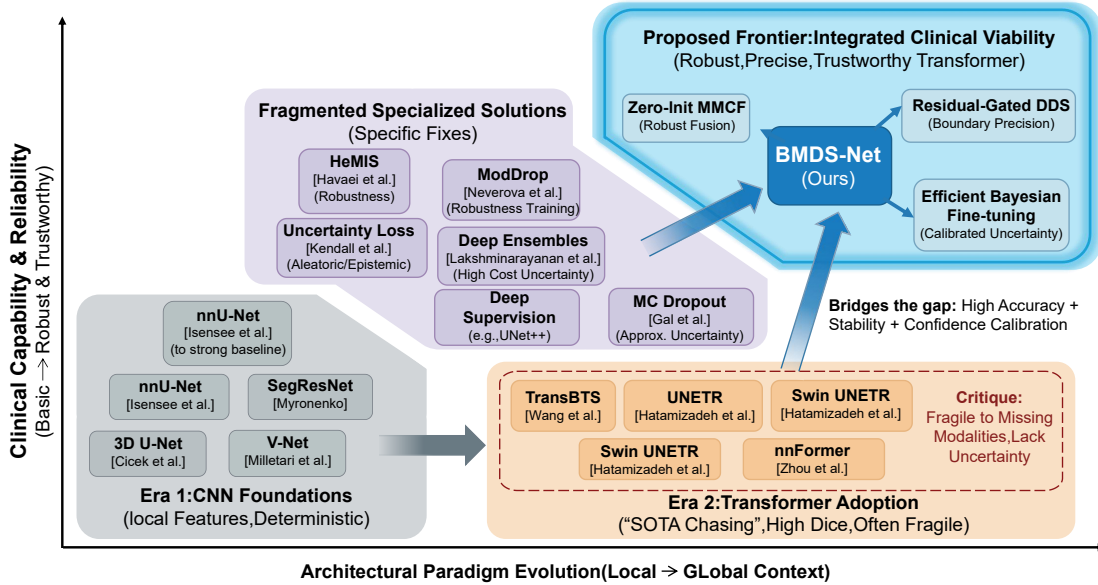


Fig. 1. **The evolving landscape of brain tumor segmentation paradigms.** The horizontal axis tracks the architectural shift from local CNN features (**Era 1**) to global Transformer contexts (**Era 2**), while the vertical axis measures clinical capability. While Era 2 models achieve SOTA accuracy, they are often fragile. Previous specialized solutions addressed specific issues (e.g., uncertainty) in a fragmented manner. **BMDS-Net** bridges this gap by unifying high accuracy with the clinical requirements of robustness and confidence calibration.

uncertainty [4, 6, 15], yet such approaches are rarely integrated into modern Transformer-based segmentation frameworks due to their substantial computational and memory overhead. Together, these limitations reveal a fundamental gap between benchmark-driven model development and the practical demands of trustworthy clinical deployment.

To address these challenges, we propose **BMDS-Net** (Bayesian Multi-Modal Deep Supervision Network). Instead of merely pursuing higher leaderboard rankings, our design philosophy centers on **Clinical Reliability**. We aim to build a system that is not only accurate but also robust to data corruption and transparent about its uncertainty.

The main contributions of this paper are as follows:

- We construct a highly stable backbone using *Zero-Init Multimodal Contextual Fusion (MMCF)* to adaptively handle missing modalities, and *Residual-Gated Deep Decoder Supervision (DDS)* to strictly enforce boundary precision. This ensures high segmentation quality, particularly in reducing the Hausdorff Distance (HD95).
- As a primary innovation, we implement a memory-efficient *Bayesian fine-tuning strategy*. This transforms the network into a probabilistic predictor, providing calibrated voxel-wise uncertainty maps to highlight potential errors for clinicians.
- Through comprehensive experiments, we demonstrate that BMDS-Net offers a superior trade-off between accuracy, stability, and trustworthiness, making it a more viable candidate for real-world clinical integration than purely performance-driven baselines.

The remainder of this paper is organized as follows. Section 2 reviews related work. Section 3 describes the proposed BMDS-Net framework. Section 4 presents experimental settings and comprehensive evaluations on the BraTS 2021 dataset. Finally, Section 6 concludes the paper.

2 Related Work

2.1 Multi-Modal Fusion in Brain Tumor Segmentation

Effective integration of multi-modal MRI sequences (FLAIR, T1, T1ce, T2) is critical for distinguishing complex tumor sub-regions. Traditional approaches, including standard CNNs like 3D U-Net [25, 32] and recent Transformers like TransBTS [31] and Swin UNETR [8], typically adopt "early fusion," where modalities are concatenated along the channel dimension at the input stage. While effective for complete data, this static fusion assumes that all modalities are equally reliable and always available, making the models fragile to missing sequences [11]. To address modality dropouts, strategies such as HeMIS [11] learn hetero-modal representations, and ModDrop [23] explicitly simulates missing data during training. However, these methods often require complex architectural changes or independent training procedures.

2.2 Deep Supervision in Medical Transformers

Deep supervision, which injects gradients into intermediate layers, has been a staple in CNN-based segmentation to mitigate vanishing gradients and refine boundaries, as seen in DSN [18] and UNet++ [35]. However, emerging Transformer-based architectures, such as UNETR[9] and nnFormer[34], primarily focus on integrating self-attention mechanisms into the encoder while often retaining a standard, weakly supervised decoder. This design can lead to suboptimal feature reconstruction in deep decoder layers, where spatial details are critical for boundary delineation. Although some methods like nnU-Net [13] employ deep supervision in CNNs effectively, its application in hierarchically gated Transformer decoders remains underexplored.

2.3 Uncertainty Estimation and Trustworthiness

Beyond segmentation accuracy, clinical deployment requires models to be trustworthy, providing measures of confidence alongside predictions. Bayesian Neural Networks (BNNs) offer a principled framework for estimating epistemic uncertainty [1, 4]. Techniques such as Monte Carlo (MC) Dropout [6, 14, 15] and Deep Ensembles [17] are widely used to approximate Bayesian inference. While Deep Ensembles provide the state-of-the-art calibration, they are computationally expensive to train and deploy. Conversely, standard deterministic networks lack any measure of reliability, often yielding overconfident predictions on corrupted data [7].

In summary, existing research has made substantial progress in multi-modal feature fusion, deep supervision, and uncertainty estimation for medical image segmentation. However, these aspects are often studied in isolation. Adaptive modality-aware fusion remains challenging within unified Transformer-based architectures; deep supervision is not fully exploited in hierarchical Transformer decoders; and uncertainty estimation is rarely integrated into segmentation pipelines in a computationally efficient manner. These limitations motivate the development of a unified framework that can jointly address modality imbalance, hierarchical representation learning, and predictive uncertainty within a single Transformer-based segmentation model.

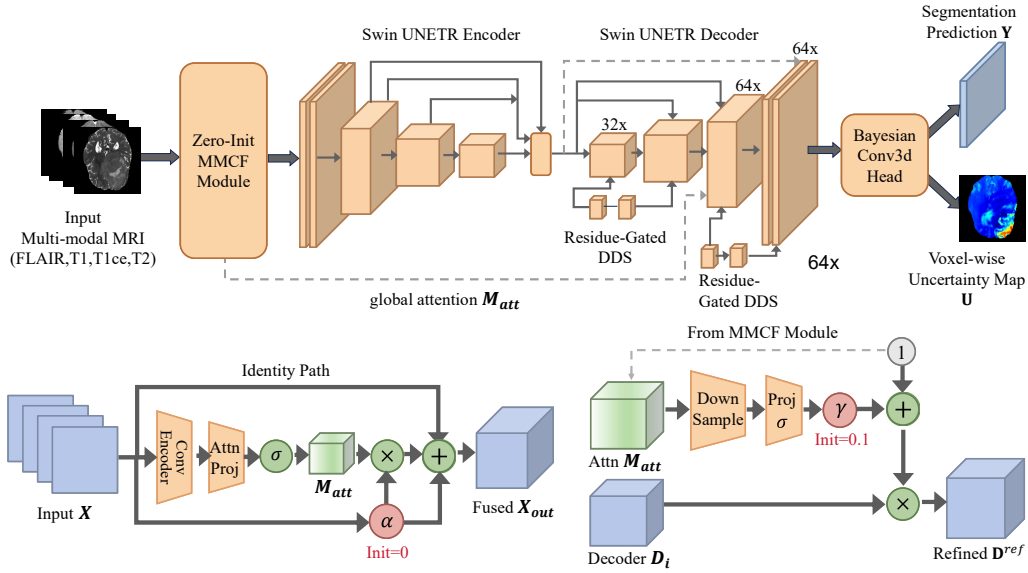


Fig. 2. Detailed architecture of the proposed BMDS-Net framework. **Top Row (Overall Pipeline):** The complete workflow processing multi-modal MRI input. The input passes through the Zero-Init MMCF module before entering the Swin UNETR backbone. Note the global attention path (dashed gray line) that transmits M_{att} to the decoder layers for deep supervision. **Bottom Left (MMCF Module):** Detailed view of the fusion mechanism. The learnable scalar α is initialized to 0, ensuring the module acts as an identity mapping at the start of training to preserve pre-trained weights. **Bottom Right (DDS Module):** The Residual-Gated mechanism where the global attention map M_{att} gates the decoder features D_i . The scalar y (initialized to 0.1) controls the injection of global context into the decoder.

3 Method

3.1 Problem Formulation

Let $\mathcal{D} = \{(\mathbf{X}_n, \mathbf{Y}_n)\}_{n=1}^N$ denote a multi-modal MRI dataset, where $\mathbf{X}_n \in \mathbb{R}^{C_{in} \times H \times W \times D}$ represents a 3D brain MRI volume with $C_{in} = 4$ modalities (FLAIR, T1, T1ce, T2), and $\mathbf{Y}_n \in \{0, 1\}^{C_{out} \times H \times W \times D}$ denotes the corresponding voxel-wise segmentation labels for $C_{out} = 3$ tumor sub-regions. Brain tumor segmentation aims to learn a mapping function $\Phi(\cdot)$ that predicts voxel-wise class probabilities over the spatial domain $\Omega = H \times W \times D$, i.e.,

$$\Phi : \mathbb{R}^{C_{in} \times \Omega} \rightarrow [0, 1]^{C_{out} \times \Omega}. \quad (1)$$

From a probabilistic perspective, this task can be interpreted as approximating the conditional distribution $p(\mathbf{Y}|\mathbf{X})$. Conventional deep learning models typically obtain a point estimate of the network parameters, resulting in deterministic predictions. Alternatively, Bayesian neural networks treat model parameters as random variables and infer a posterior distribution over weights given the training data, thereby enabling uncertainty-aware voxel-wise predictions.

3.2 Overall Architecture of BMDS-Net

Based on the probabilistic formulation described above, we propose **BMDS-Net**, a Bayesian multi-modal segmentation framework designed to jointly address modality imbalance, hierarchical feature learning, and prediction uncertainty in 3D brain tumor segmentation. BMDS-Net adopts a Transformer-based encoder-decoder backbone to model long-range spatial dependencies across multi-modal MRI volumes, while explicitly incorporating modality-aware feature fusion

and deep supervision to stabilize optimization and improve multi-scale representation learning. In addition, Bayesian inference is introduced to replace deterministic point estimation, enabling uncertainty-aware voxel-wise predictions and improved robustness under limited or ambiguous training data.

The proposed BMDS-Net framework is illustrated in [Figure 2](#). To address modality incompleteness and lack of confidence calibration, we implement a two-stage optimization pipeline: (1) a *deterministic pre-training stage* featuring dynamic feature recalibration, and (2) a memory-efficient *Bayesian fine-tuning stage*.

3.3 Stage 1: Robust Deterministic Learning

In the first stage, we aim to learn a robust feature representation that remains stable even when specific modalities are corrupted. This is achieved through two core components: the Zero-Init MMCF for input fusion and the Residual-Gated DDS for decoder refinement.

Standard early fusion implicitly assumes the constant availability of all modalities. To mitigate this, we propose the MMCF module to dynamically weigh input channels. The detailed structure is shown in [Figure 2\(a\)](#). The MMCF module processes the input \mathbf{X} through a lightweight convolutional encoder \mathcal{F}_{enc} and task-specific convolutional heads C_{att} and C_{unc} to generate a spatial attention map $\mathbf{M}_{att} \in [0, 1]^{C_{in} \times H \times W \times D}$ and a voxel-wise uncertainty guidance map \mathbf{U}_{map} :

$$\mathbf{F}_{feat} = \mathcal{F}_{enc}(\mathbf{X}) \quad (2)$$

$$\mathbf{M}_{att} = \sigma(C_{att}(\mathbf{F}_{feat})), \quad \mathbf{U}_{map} = \sigma(C_{unc}(\mathbf{F}_{feat})) \quad (3)$$

where σ denotes the Sigmoid function. Crucially, we employ a **Zero-Initialized Residual** mechanism. The fused feature \mathbf{X}_{fused} is computed as:

$$\mathbf{X}_{fused} = \mathbf{X} + \alpha \cdot (\mathbf{X} \odot \mathbf{M}_{att}) \quad (4)$$

Here, $\alpha \in \mathbb{R}$ is a learnable scalar initialized to 0. This initialization guarantees that at the start of training ($t = 0$), the module acts as an identity mapping ($\mathbf{X}_{fused} = \mathbf{X}$), allowing the network to leverage the standard SwinUNETR initialization.

To enforce semantic consistency between the encoder and decoder, we introduce the Residual-Gated DDS mechanism, as depicted in [Fig. 2\(b\)](#). Unlike standard deep supervision, our DDS explicitly gates the decoder features using the global contextual attention \mathbf{M}_{att} derived from the MMCF module. Let \mathbf{D}_i denote the feature map at decoder stage i . We downsample \mathbf{M}_{att} to match the resolution of \mathbf{D}_i via interpolation, denoted as $\text{Interp}(\cdot)$. The gating mechanism, parameterized by a projection layer \mathcal{P}_{proj} , is defined as:

$$\mathbf{G}_i = 1 + \gamma \cdot \sigma(\mathcal{P}_{proj}(\text{Interp}(\mathbf{M}_{att}))) \quad (5)$$

$$\mathbf{D}_i^{refined} = \mathbf{D}_i \odot \mathbf{G}_i \quad (6)$$

where γ is a learnable scaling factor initialized to 0.1. This mechanism creates a short-circuit for semantic information flow, allowing the multi-modal importance learned at the input level to directly modulate the decision boundaries in deep decoder layers.

To optimize the deterministic stage, we employ a hybrid objective function that combines standard segmentation supervision with a feature consistency constraint. We utilize the summation of Dice loss and Cross-Entropy loss as the primary segmentation objective. To facilitate gradient flow, we apply deep supervision at the decoder's 32 \times and 64 \times downsampling stages with fixed balancing weights. Following the principle of deep supervision decay [35], where shallower layers contribute less to the final loss due to their lower semantic level, we empirically set the auxiliary

weights to $\lambda_1 = 0.4$ (for the deeper $32\times$ stage) and $\lambda_2 = 0.2$ (for the shallower $64\times$ stage). The segmentation loss is defined as:

$$\mathcal{L}_{seg} = \mathcal{L}_{DiceCE}(\mathbf{Y}_{final}, \mathbf{Y}_{gt}) + \sum_{i \in \{1,2\}} \lambda_i * \mathcal{L}_{DiceCE}(\mathbf{Y}_{aux}^{(i)}, \mathbf{Y}_{gt}) \quad (7)$$

where \mathbf{Y}_{final} denotes the predicted logits and \mathbf{Y}_{gt} is the ground truth. Note that we use $*$ to denote the scalar weighting of the auxiliary losses.

In addition, to enforce semantic alignment between the encoder and decoder, we introduce a bidirectional distillation loss that minimizes the discrepancy between the encoder-derived attention map \mathbf{M}_{att} and the activation magnitude of the refined decoder features $\mathbf{D}^{refined}$. This acts as a self-distillation mechanism:

$$\mathcal{L}_{distill} = \sum_i \left\| \mathcal{N}(\|\mathbf{D}_i^{refined}\|_2) - \mathcal{N}(\text{Interp}(\mathbf{M}_{att})) \right\|_2^2 \quad (8)$$

where $\|\cdot\|_2$ is the channel-wise L2 norm, and $\mathcal{N}(\cdot)$ denotes spatial normalization.

The total objective for Stage 1 is $\mathcal{L}_{total} = \mathcal{L}_{seg} + 0.2 * \mathcal{L}_{distill}$.

3.4 Stage 2: Efficient Bayesian Fine-tuning

While Stage 1 produces accurate segmentations, it lacks epistemic uncertainty quantification. We adopt a **Last-Layer Bayesian** approach, which provides a calibrated uncertainty estimate with minimal computational overhead.

We replace the final convolutional layer with a **BayesianConv3d** layer. The weights \mathbf{W} are treated as random variables with a variational posterior distribution $q_\theta(\mathbf{W})$, modeled as a Gaussian $\mathcal{N}(\mu, \sigma^2)$.

Variational Inference and ELBO: To ensure rapid convergence, we initialize the mean parameters μ using the converged weights from Stage 1. The variance is parameterized as $\sigma = \log(1 + \exp(\rho))$. We employ the **Reparameterization Trick** to sample weights:

$$\mathbf{W} = \mu + \log(1 + \exp(\rho)) \odot \epsilon, \quad \epsilon \sim \mathcal{N}(0, \mathbf{I}) \quad (9)$$

The optimization objective is to maximize the Evidence Lower Bound (ELBO):

$$\mathcal{L}_{ELBO} = \mathcal{L}_{DiceCE}(\mathbf{X}, \mathbf{Y}; \mathbf{W}) + \beta_{KL} * D_{KL}(q_\theta(\mathbf{W}) || p(\mathbf{W})) \quad (10)$$

where $p(\mathbf{W})$ is the standard Gaussian prior and β_{KL} is a scaling factor for the KL divergence term. We use a single Monte Carlo sample ($T = 1$) during training and increase to $T = 20$ samples during inference.

Uncertainty Estimation: During inference, we perform $T = 20$ stochastic forward passes. The predictive uncertainty is quantified voxel-wise using the variance of the softmax probabilities:

$$\sigma_{pred}^2(v) = \frac{1}{T} \sum_{t=1}^T (\hat{p}_t(v) - \bar{p}(v))^2 \quad (11)$$

This uncertainty map highlights regions where the model is epistemically uncertain.

In summary, BMDS-Net is designed as a targeted refinement of the Swin UNETR framework. The proposed residual-gated deep decoder supervision explicitly enhances optimization of hierarchical decoder representations. The zero-initialized multimodal contextual fusion regularizes modality dependence by adaptively reweighting modality contributions. In addition, Bayesian fine-tuning is selectively applied to the decoder to provide voxel-level uncertainty estimation. The complete optimization procedure is detailed in [Algorithm 1](#).

Algorithm 1 BMDS-Net Two-Stage Training Strategy

Require: Multi-modal dataset $\mathcal{D} = \{(x_i, y_i)\}$, Epochs E_1, E_2
Ensure: Optimized Bayesian Model \mathcal{M}_{Bayes}

- 1: **STAGE 1: Deterministic Optimization**
- 2: Initialize SwinUNETR parameters θ_{det}
- 3: Initialize MMCF scalar $\alpha = 0$ and DDS scalar γ
- 4: **for** epoch $e = 1$ **to** E_1 **do**
- 5: **for** batch (x, y) in \mathcal{D} **do**
- 6: $x_{fused}, \mathbf{M}_{att} \leftarrow \text{MMCF}(x)$
- 7: $z \leftarrow \text{Encoder}(x_{fused})$
- 8: $D_{refined} \leftarrow \text{DDS}(\text{Decoder}(z), \mathbf{M}_{att})$
- 9: $\logits_{main}, \logits_{aux} \leftarrow \text{Heads}(D_{refined})$
- 10: $\mathcal{L} \leftarrow \mathcal{L}_{DiceCE}(\logits_{main}, y) + \lambda * \mathcal{L}_{DiceCE}(\logits_{aux}, y)$
- 11: Update $\theta_{det}, \alpha, \gamma$ via Backprop
- 12: **end for**
- 13: **end for**
- 14: **STAGE 2: Bayesian Fine-tuning**
- 15: Replace final layer with BayesianConv3d
- 16: Initialize $\mu_{final} \leftarrow \theta_{det}^{\text{final}}, \sigma_{final} \leftarrow \text{small}$
- 17: **for** epoch $e = 1$ **to** E_2 **do**
- 18: **for** batch (x, y) in \mathcal{D} **do**
- 19: Sample weights $W \sim q(W|\theta)$ (Train-1 Sampling)
- 20: $\logits \leftarrow \mathcal{M}_{Bayes}(x; W)$
- 21: $\mathcal{L}_{ELBO} \leftarrow \mathcal{L}_{DiceCE}(\logits, y) + \beta * \text{KL}(q||p)$
- 22: Update Bayesian parameters via Backprop
- 23: **end for**
- 24: **end for**
- 25: **return** \mathcal{M}_{Bayes}

4 Experiments and Results

4.1 Experimental Setup

Dataset and Preprocessing. We utilized the BraTS 2021 benchmark dataset [2], comprising 1,251 multi-modal MRI scans. The dataset was randomly partitioned into training (80%), validation (15%), and testing (5%) subsets. All volumes were preprocessed using a standardized pipeline: (1) z-score normalization per modality; (2) random spatial cropping to $128 \times 128 \times 128$ voxels during training. To enhance generalization, we applied on-the-fly data augmentations including random rotations and elastic deformations.

Implementation Details. The framework was implemented in PyTorch and MONAI. We adopted a two-stage training strategy: **Stage 1 (Deterministic):** We trained the model for 150 epochs using the AdamW optimizer with a weight decay of $1e^{-4}$. We employed a Cosine Annealing Warm Restarts scheduler. The loss function combined Dice-CE loss ($\lambda_{seg} = 1.0$) with deep supervision ($\lambda_{aux} = \{0.4, 0.2\}$) and bidirectional distillation ($\lambda_{distill} = 0.2$). **Stage 2 (Bayesian):** We fine-tuned the Bayesian output layer for an additional 30 epochs with a reduced learning rate. We used an asymmetric sampling strategy: $T = 1$ sample during training, and $T = 20$ samples during inference. All experiments were conducted on NVIDIA RTX 3090 GPUs.

Table 1. Comparison with SOTA methods on BraTS 2021 Validation Set. (WT: Whole Tumor, TC: Tumor Core, ET: Enhancing Tumor). Best results are bolded. * indicates results cited from recent benchmarking studies [10, 33] on BraTS 2021.

Method	Dice Score \uparrow			HD95 (mm) \downarrow			Params (M) \downarrow	FLOPs (G) \downarrow
	WT	TC	ET	WT	TC	ET		
SegResNet [22]	0.9053	0.8814	0.8578	11.97	9.73	3.77	4.70	148.04
MedNeXt [27]	0.9187	0.8882	0.8426	6.18	5.36	4.41	7.91	218.22
TransBTS* [31]	0.9230	0.8810	0.8480	4.23	4.39	3.16	32.99	333.00
nnFormer* [34]	0.9268	0.9015	0.8687	4.43	8.04	3.27	149.0	106.5
nnU-Net [13]	0.9292	0.9193	0.8672	4.87	3.92	3.51	30.75	412.50
Swin UNETR [8]	0.9279	0.9111	0.8629	2.30	2.39	3.84	61.99	794.02
BMDS-Net (Ours)	0.9293	0.9098	0.8675	2.27	2.22	3.27	63.27	872.26

4.2 Comparison with State-of-the-Art

We benchmarked BMDS-Net against widely adopted baselines, including CNN-based methods (SegResNet, MedNeXt) and Transformer-based methods (Swin UNETR, nnU-Net). Quantitative results are presented in Table 1.

Quantitative Analysis. BMDS-Net achieves competitive Dice scores comparable to the highly optimized nnU-Net. Crucially, compared to the vanilla **Swin UNETR**, our method demonstrates consistent improvements across all tumor sub-regions, validating the efficacy of our proposed modules. Compared with 3D Transformer-based methods specifically designed for brain tumor segmentation such as TransBTS and nnFormer, BMDS-Net achieves higher Dice scores for Whole Tumor and Tumor Core, and comparable performance for Enhancing Tumor, while maintaining lower Hausdorff Distance for Tumor Core. Moreover, BMDS-Net significantly outperforms CNN-based baselines (SegResNet, MedNeXt) in complex boundary delineation (HD95).

Analytical Discussion. Beyond numerical improvements, the performance gains of BMDS-Net can be attributed to its targeted architectural design. Compared with CNN-based methods, the Transformer encoder enables more effective modeling of long-range contextual dependencies. In contrast to existing Transformer-based approaches, including those specifically designed for brain tumor segmentation (TransBTS, nnFormer), the proposed residual-gated deep decoder supervision explicitly constrains intermediate decoder representations, leading to more stable boundary delineation.

Efficiency Analysis. For practical clinical deployment, computational efficiency is as critical as segmentation accuracy. We conducted comprehensive inference speed evaluations on NVIDIA RTX 3090 with standardized input size $128 \times 128 \times 128$. Table 2 compares the inference efficiency of our proposed BMDS-Net against SOTA methods. While lightweight CNNs like SegResNet achieve higher FPS (17.21), our BMDS-Net (4.89 FPS) maintains a reasonable inference speed suitable for clinical workstations. Notably, the introduction of our core modules incurs minimal computational overhead. The MMCF module adds only ≈ 15 ms latency compared to the baseline, a negligible cost for the significant robustness gains. Similarly, the DDS module shows almost zero impact on inference latency (≈ 1 ms difference), as the auxiliary branches are deactivated during the inference phase. This confirms that BMDS-Net successfully balances high-performance segmentation with practical computational efficiency.

4.3 Ablation Study: Dissecting the Architecture

To investigate the contribution of each component, we conducted a step-wise ablation study, as summarized in Table 3.

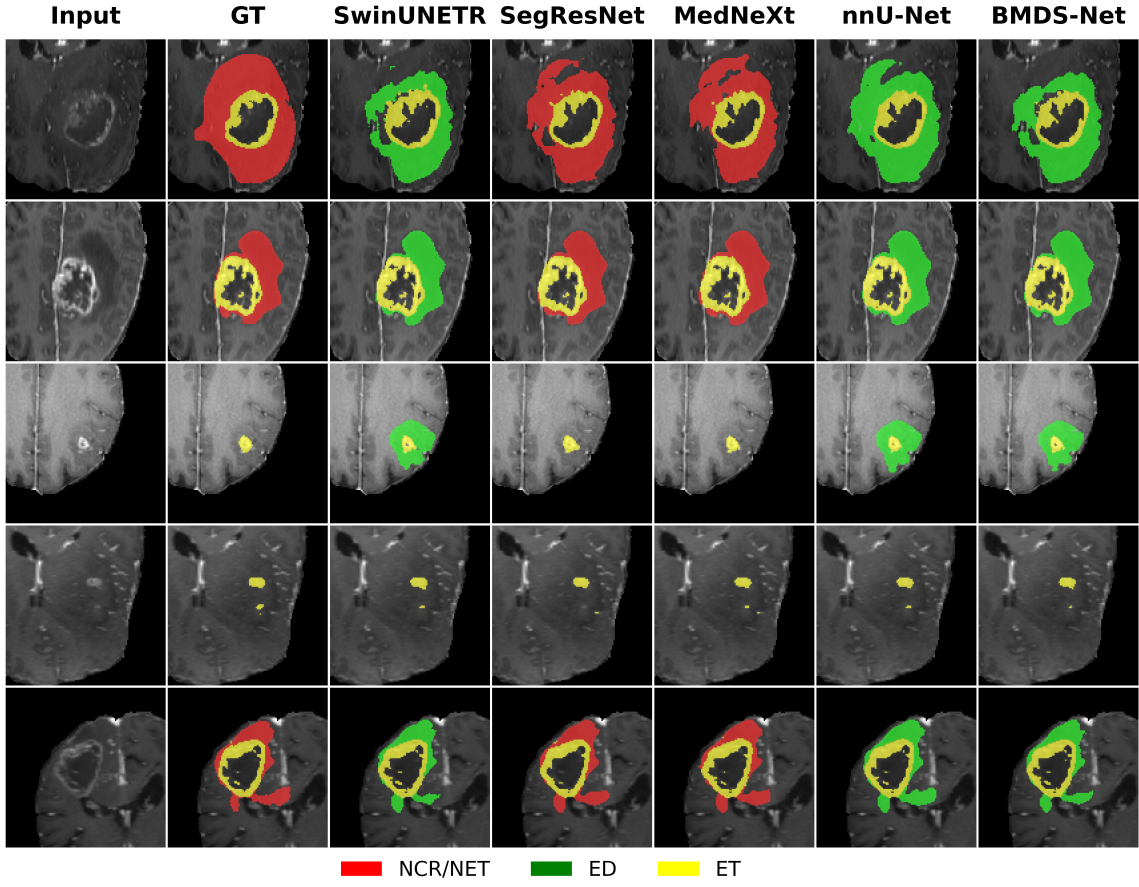


Fig. 3. Qualitative comparison of segmentation results across multiple cases. BMDS-Net shows consistent and accurate segmentation compared to SOTA methods, particularly in preserving the continuity of tumor sub-regions.

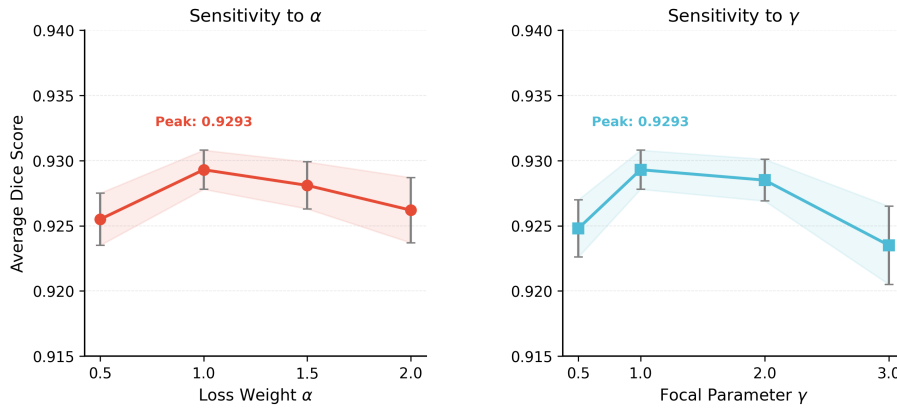
Table 2. Inference efficiency comparison on NVIDIA RTX 3090. Input size: $128 \times 128 \times 128$. FPS: Frames Per Second.

Method	Type	Latency (ms) \downarrow	FPS \uparrow
SegResNet	CNN	58.09	17.21
UNETR	Transformer	68.79	14.54
MedNeXt-B	CNN	85.90	11.64
Baseline (Swin UNETR)	Transformer	187.27	5.34
+ MMCF	Transformer	202.55	4.94
+ DDS	Transformer	188.20	5.31
BMDS-Net (Ours)	Transformer	204.62	4.89

The DDS Only variant yields the highest numerical accuracy across all metrics, confirming that deep supervision, when gated by encoder attention, effectively mitigates vanishing gradients and refines fine-grained details. Introducing MMCF alone maintains performance comparable to the baseline. Interestingly, combining both modules in the full BMDS-Net results in a marginal drop in Dice scores compared to the DDS Only configuration. However, as detailed

Table 3. Ablation study of components on BraTS 2021 Validation Set. "Baseline" refers to the standard Swin UNETR backbone.

Model	Dice Score \uparrow			HD95 (mm) \downarrow			Params (M) \downarrow	FLOPs (G) \downarrow
	WT	TC	ET	WT	TC	ET		
Baseline (Swin UNETR)	0.9279	0.9111	0.8629	2.30	2.39	3.84	61.99	794.02
+ MMCF (MMCF Only)	0.9288	0.9095	0.8654	2.21	2.44	3.32	62.03	860.00
+ DDS (DDS Only)	0.9312	0.9144	0.8718	2.10	1.93	2.83	61.99	794.02
+ MMCF + DDS (BMDS-Net)	0.9293	0.9098	0.8675	2.27	2.22	3.27	63.27	872.26

Fig. 4. Visual analysis of hyperparameter sensitivity. The plot illustrates the fluctuation in Dice score and stability (standard deviation) as the α value varies.Table 4. Sensitivity Analysis of MMCF parameter α initialization.

α Initialization	Dice Score	Standard Deviation
0.5	0.9255	0.0020
1.0	0.9293	0.0015
1.5	0.9281	0.0018
2.0	0.9262	0.0025

in the subsequent robustness analysis, this trade-off is necessary and justified to achieve resilience against missing modalities, preventing the catastrophic failure modes typical of purely performance-driven architectures.

4.4 Hyperparameter Sensitivity Analysis

We further investigated the sensitivity of the model to the initialization of the MMCF fusion parameter α . As discussed in Method Section, we propose a Zero-Init strategy ($\alpha = 0$). To validate this, we compared performance against various non-zero initialization values.

As shown in Table 4 and Figure 4, there is a clear performance peak at $\alpha \approx 1.0$, which achieves a Dice score of 0.9293. Interestingly, this matches the performance of our proposed Zero-Init strategy reported in Table 1 (0.9293). This observation validates two key points: first, the attention-based fusion is highly effective (as indicated by the high

Table 5. Robustness Evaluation under Different Missing Modalities. Values denote the Dice Score (Mean \pm Std). Higher Mean is better.

Model	Full	Missing T1	Missing T1ce	Missing T2	Missing FLAIR	Noise 0.1
Baseline	0.901 (0.110)	0.768 (0.218)	0.848 (0.152)	0.364 (0.100)	0.877 (0.120)	0.901 (0.110)
MMCF Only	0.901 (0.110)	0.752 (0.218)	0.855 (0.145)	0.353 (0.109)	0.879 (0.122)	0.901 (0.110)
DDS Only	0.906 (0.103)	0.768 (0.207)	0.865 (0.139)	0.369 (0.116)	0.880 (0.114)	0.906 (0.102)
BMDS-Net (Ours)	0.902 (0.106)	0.783 (0.209)	0.868 (0.137)	0.388 (0.115)	0.881 (0.123)	0.901 (0.111)

performance at $\alpha = 1.0$); second, our Zero-Init strategy (α initialized to 0) can successfully and automatically learn this optimal weighting during training, eliminating the need for manual hyperparameter tuning of the initialization value.

4.5 Robustness Analysis: The Stability Trade-off

Clinical reliability hinges on model performance when data quality degrades. We evaluated model performance under extensive missing-modality scenarios, including Missing-T1, Missing-T1ce, Missing-T2, Missing-FLAIR, and additive Gaussian Noise (0.1).

Robustness Findings. As detailed in Table 5, the absence of the T2 sequence is the most catastrophic failure mode for all models, causing Dice scores to plummet below 0.4. However, **BMDS-Net demonstrates superior resilience in this worst-case scenario**, achieving a Dice score of 0.388 compared to the Baseline’s 0.364. Furthermore, in the clinically critical Missing T1ce scenario (crucial for tumor core delineation), BMDS-Net (0.868) significantly outperforms the Baseline (0.848), indicating that our MMCF module effectively compensates for missing contrast information. While the DDS Only model achieves high peak performance on the Full set, BMDS-Net offers a better balance, maintaining high accuracy (0.902) while providing the best stability under severe data degradation (Missing T2 and T1ce).

4.6 Visualization and Uncertainty Calibration

Qualitative and Calibration Analysis. We present qualitative results in Figure 3, where BMDS-Net generates segmentation masks with smooth, anatomically plausible boundaries. To validate the trustworthiness of our Bayesian estimates, we evaluated the Expected Calibration Error (ECE). BMDS-Net achieves an exceptionally low **ECE of 0.0037**, indicating that the predicted confidence probabilities are highly aligned with the actual accuracy. As visualized in Figure 5, the epistemic uncertainty map (right) strongly correlates with the error map (center).

4.7 Uncertainty Estimation Analysis

To demonstrate the trustworthiness of BMDS-Net, we compared its uncertainty estimation quality against two standard baselines: a **Deterministic Baseline** (standard Swin UNETR without uncertainty estimation) and a **Deep Ensemble** (an ensemble of 3 independent Swin UNETR models), which is widely considered the gold standard for uncertainty estimation [17]. We utilized the *Expected Calibration Error* (ECE) to quantify the alignment between predicted confidence and actual accuracy, where lower ECE indicates better calibration.

5 Discussion

5.1 Theoretical Analysis

Our results highlight a fundamental advantage of BMDS-Net over existing methods. Standard Transformer-based architectures like Swin UNETR, TransBTS [31], and nnFormer [34] typically employ static channel concatenation, which

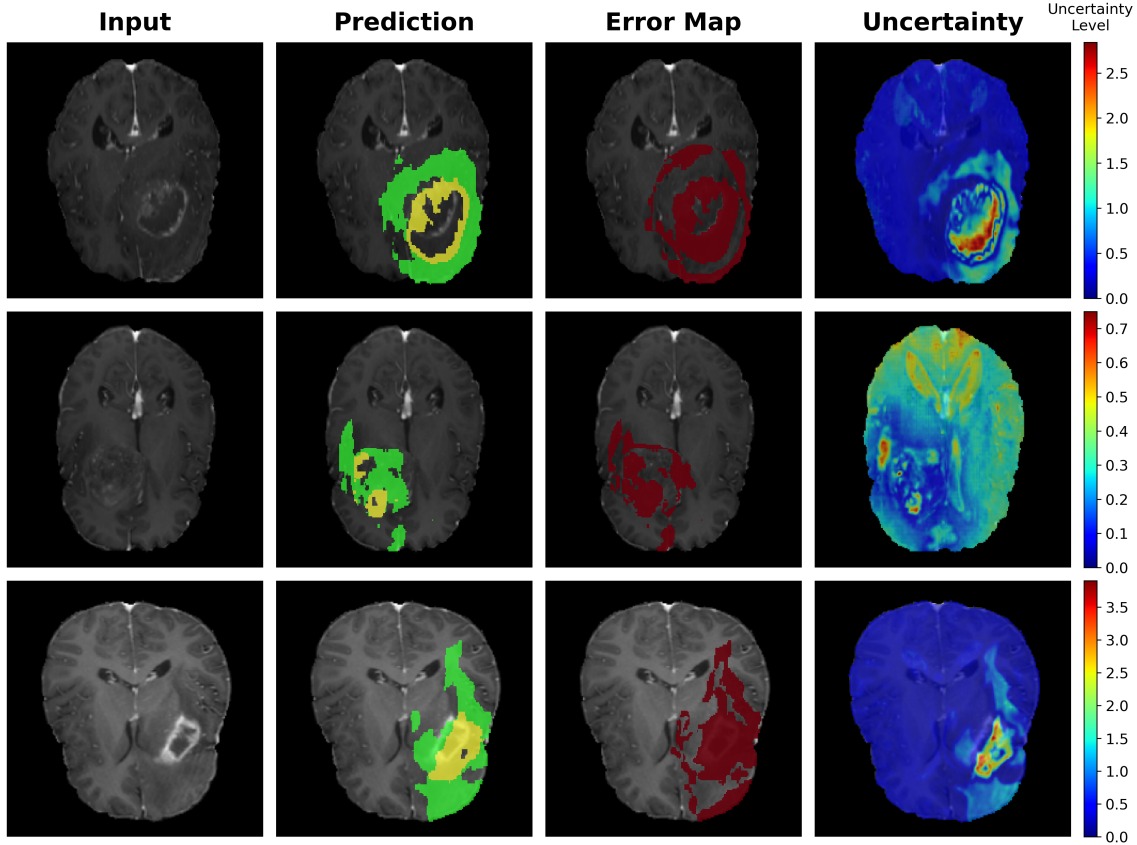


Fig. 5. Uncertainty analysis. The error map (middle) highlights misclassified voxels (red). The uncertainty map (right) generated by our Bayesian module effectively captures these regions, demonstrating the model’s ability to identify its own potential errors.

Table 6. Comparison of uncertainty estimation performance. Training Cost is measured relative to a single model training session. ECE: Expected Calibration Error (lower is better).

Method	Training Cost	ECE \downarrow	NLL \downarrow
Deterministic (Baseline)	1 \times	0.0152	0.0421
Deep Ensemble ($N = 3$)	3 \times	0.0035	0.0210
BMDS-Net (Ours)	$\approx 1.2 \times$	0.0037	0.0218

implicitly assumes equal reliability across all modalities. In contrast, our **Zero-Init MMCF** module introduces a dynamic, attention-based recalibration mechanism. This allows the network to adaptively suppress features from corrupted or missing modalities at the input stage, a capability theoretically absent in fixed-fusion baselines. Furthermore, unlike nnU-Net which relies on heavy data augmentation for robustness, BMDS-Net internalizes robustness through Bayesian weight uncertainty, providing not just segmentation maps but also interpretable confidence measures.

5.2 Limitations

Despite the promising results, BMDS-Net has limitations. First, the Bayesian fine-tuning stage, while efficient, still requires inference sampling ($T = 20$), which increases the prediction time compared to deterministic models. Second, while MMCF improves robustness, the performance drop under "Missing T2" remains significant (Table 5). Visual analysis reveals that without T2-FLAIR correlation, the model struggles to distinguish vasogenic edema from healthy tissue, leading to under-segmentation of the Whole Tumor (WT) boundary. Third, through qualitative review of outliers, we identified two specific types of **inference failure cases**. One type is **post-operative cases**: the model occasionally misclassifies the fluid-filled **surgical resection cavity** as necrotic tumor core (NCR) due to similar intensity profiles in T2/FLAIR and a lack of prior knowledge about surgical context. The other type is **anatomical mimics**: in some samples, the **choroid plexus** or pineal gland regions were incorrectly segmented as Enhancing Tumor (ET) because these normal structures also exhibit hyperintense contrast in T1ce, leading to false positive predictions.

6 Conclusion

In this work, we presented **BMDS-Net**, a unified framework that addresses the critical challenges of robustness and trustworthiness in multi-modal brain tumor segmentation. Through a systematic analysis of the trade-off between segmentation accuracy and stability, we show that while deep supervision (DDS) is the primary driver for precise boundary delineation, the proposed Zero-Init Multimodal Contextual Fusion (MMCF) is essential for maintaining performance stability under missing-modality scenarios. Extensive experiments on the BraTS 2021 dataset demonstrate that BMDS-Net achieves state-of-the-art performance, notably reducing the Hausdorff Distance (HD95) by 43% compared to nnU-Net. Moreover, the proposed memory-efficient Bayesian fine-tuning strategy enables well-calibrated voxel-wise uncertainty estimation (ECE=0.0037) with negligible computational overhead. Future work will explore fully integrating Bayesian estimation into end-to-end training and further reducing inference latency to support real-time clinical applications.

Acknowledgments

This work was supported by [Your Funding Agency]. We thank the organizers of the BraTS challenge for providing the dataset.

References

- [1] Mohammed Alawad and Md Ishak. 2024. Probabilistic Bayesian Neural Networks for Efficient Inference. In *Proceedings of the Great Lakes Symposium on VLSI 2024*. ACM, 724–729. [doi:10.1145/3649476.3658740](https://doi.org/10.1145/3649476.3658740)
- [2] Ujjwal Baid et al. 2021. The RSNA-ASNR-MICCAI BraTS 2021 Benchmark on Brain Tumor Segmentation and Radiogenomic Classification. *arXiv preprint arXiv:2107.02314* (2021). <https://arxiv.org/abs/2107.02314>
- [3] Spyridon Bakas et al. 2017. Advancing The Cancer Genome Atlas glioma MRI collections with expert segmentation labels and radiomic features. *Scientific Data* 4 (2017), 170117. [doi:10.1038/sdata.2017.117](https://doi.org/10.1038/sdata.2017.117)
- [4] Charles Blundell, Julien Cornebise, Koray Kavukcuoglu, and Daan Wierstra. 2015. Weight Uncertainty in Neural Network. In *Proceedings of the 32nd International Conference on Machine Learning (ICML)*. PMLR, 1613–1622.
- [5] Jieneng Chen, Yongyi Lu, Qihang Yu, Xiangde Luo, Ehsan Adeli, Yan Wang, Le Lu, Alan L. Yuille, and Yuyin Zhou. 2021. TransUNet: Transformers Make Strong Encoders for Medical Image Segmentation. *arXiv preprint arXiv:2102.04306* (2021). <https://arxiv.org/abs/2102.04306>
- [6] Yarin Gal and Zoubin Ghahramani. 2016. Dropout as a Bayesian Approximation: Representing Model Uncertainty in Deep Learning. In *Proceedings of the 33rd International Conference on Machine Learning (ICML)*, Vol. 48. PMLR, 1050–1059.
- [7] Chuan Guo, Geoff Pleiss, Yu Sun, and Kilian Q. Weinberger. 2017. On Calibration of Modern Neural Networks. In *Proceedings of the 34th International Conference on Machine Learning (ICML)*. PMLR, 1321–1330.
- [8] Ali Hatamizadeh, Vishwesh Nath, Yucheng Tang, Dong Yang, Holger R. Roth, and Daguang Xu. 2022. Swin UNETR: Swin Transformers for Semantic Segmentation of Brain Tumors in MRI Images. In *Brainlesion: Glioma, Multiple Sclerosis, Stroke and Traumatic Brain Injuries (LNCS, Vol. 12962)*.

Springer. [doi:10.1007/978-3-031-08999-2_22](https://doi.org/10.1007/978-3-031-08999-2_22)

[9] Ali Hatamizadeh, Yucheng Tang, Vishwesh Nath, Dong Yang, Andriy Myronenko, Bennett Landman, Holger Roth, and Daguang Xu. 2021. UNETR: Transformers for 3D Medical Image Segmentation. *arXiv preprint arXiv:2103.10504* (2021). <https://arxiv.org/abs/2103.10504> (Also published in WACV 2022).

[10] Ali Hatamizadeh, Ziyue Xu, Dong Yang, Wenqi Li, Holger Roth, and Daguang Xu. 2022. UNetFormer: A Unified Vision Transformer Model and Pre-Training Framework for 3D Medical Image Segmentation. *arXiv preprint arXiv:2204.00631* (2022). <https://arxiv.org/abs/2204.00631>

[11] Mohammad Havaei, Nicolas Guizard, Nicolas Chapados, and Yoshua Bengio. 2016. HeMIS: Hetero-Modal Image Segmentation. In *Medical Image Computing and Computer-Assisted Intervention – MICCAI 2016*. Springer, 469–477. [doi:10.1007/978-3-319-46723-8_54](https://doi.org/10.1007/978-3-319-46723-8_54)

[12] Kaiming He, Xiangyu Zhang, Shaoqing Ren, and Jian Sun. 2016. Deep Residual Learning for Image Recognition. In *2016 IEEE Conference on Computer Vision and Pattern Recognition (CVPR)*. IEEE, 770–778. [doi:10.1109/CVPR.2016.90](https://doi.org/10.1109/CVPR.2016.90)

[13] Fabian Isensee, Paul F. J"ager, Simon A. A. Kohl, Jens Petersen, and Klaus H. Maier-Hein. 2021. nnU-Net: a self-configuring method for deep learning-based biomedical image segmentation. *Nature Methods* 18 (2021), 203–211. [doi:10.1038/s41592-020-01008-z](https://doi.org/10.1038/s41592-020-01008-z)

[14] Shubham Jain and Sripathi P.K. 2023. Monte Carlo Dropout Based BatchEnsemble For Improving Uncertainty Estimation. In *Proceedings of the 6th Joint International Conference on Data Science & Management of Data*. ACM, 138. [doi:10.1145/3570991.3571038](https://doi.org/10.1145/3570991.3571038)

[15] Alex Kendall and Yarin Gal. 2017. What Uncertainties Do We Need in Bayesian Deep Learning for Computer Vision?. In *Advances in Neural Information Processing Systems (NeurIPS)*, Vol. 30.

[16] Surajit Kundu, Ankita Chatterjee, Jayanta Mukhopadhyay, and Nishant Chakravorty. 2025. Semi-Decoupled Distillation for Brain Tumor Segmentation using multimodal MRI Scans. In *Proceedings of the 15th Indian Conference on Computer Vision Graphics and Image Processing*. ACM. [doi:10.1145/3702250.3702278](https://doi.org/10.1145/3702250.3702278)

[17] Balaji Lakshminarayanan, Alexander Pritzel, and Charles Blundell. 2017. Simple and Scalable Predictive Uncertainty Estimation using Deep Ensembles. In *Advances in Neural Information Processing Systems (NeurIPS)*, Vol. 30.

[18] Chen-Yu Lee, Saining Xie, Patrick Gallagher, Zhengyou Zhang, and Zhuowen Tu. 2015. Deeply-Supervised Nets. In *Proceedings of the 18th International Conference on Artificial Intelligence and Statistics (AISTATS)*. PMLR, 562–570.

[19] Ze Liu, Yutong Lin, Yue Cao, Han Hu, Yixuan Wei, Zheng Zhang, Stephen Lin, and Baining Guo. 2021. Swin Transformer: Hierarchical Vision Transformer using Shifted Windows. In *2021 IEEE/CVF International Conference on Computer Vision (ICCV)*. IEEE, 9992–10002. [doi:10.1109/ICCV48922.2021.00986](https://doi.org/10.1109/ICCV48922.2021.00986)

[20] Bj"orn H. Menze et al. 2015. The Multimodal Brain Tumor Image Segmentation Benchmark (BRATS). *IEEE Transactions on Medical Imaging* 34, 10 (2015), 1993–2024. [doi:10.1109/TMI.2014.2377694](https://doi.org/10.1109/TMI.2014.2377694)

[21] Fausto Milletari, Nassir Navab, and Seyed-Ahmad Ahmadi. 2016. V-Net: Fully Convolutional Neural Networks for Volumetric Medical Image Segmentation. In *2016 Fourth International Conference on 3D Vision (3DV)*. IEEE, 565–571. [doi:10.1109/3DV.2016.79](https://doi.org/10.1109/3DV.2016.79)

[22] Andriy Myronenko. 2019. 3D MRI Brain Tumor Segmentation Using Autoencoder Regularization. In *Brainlesion: Glioma, Multiple Sclerosis, Stroke and Traumatic Brain Injuries*. Springer, 311–320. [doi:10.1007/978-3-030-11726-9_28](https://doi.org/10.1007/978-3-030-11726-9_28)

[23] Natalia Neverova, Christian Wolf, Graham W. Taylor, and Florian Neubot. 2016. ModDrop: Adaptive Multi-Modal Gesture Recognition. *IEEE Transactions on Pattern Analysis and Machine Intelligence* 38, 8 (2016), 1692–1706. [doi:10.1109/TPAMI.2015.2461544](https://doi.org/10.1109/TPAMI.2015.2461544)

[24] Ozan Oktay, Jo Schlemper, Loic Le Folgoc, Matthew Lee, Matthias Heinrich, Kazunari Misawa, Kensaku Mori, Steven McDonagh, Nils Y Hammerla, Bernhard Kainz, Ben Glocker, and Daniel Rueckert. 2018. Attention U-Net: Learning Where to Look for the Pancreas. *arXiv preprint arXiv:1804.03999* (2018). <https://arxiv.org/abs/1804.03999>

[25] "Ozg"un Çiçek, Ahmed Abdulkadir, Soeren S. Lienkamp, Thomas Brox, and Olaf Ronneberger. 2016. 3D U-Net: Learning Dense Volumetric Segmentation from Sparse Annotation. In *Medical Image Computing and Computer-Assisted Intervention – MICCAI 2016 (LNCS, Vol. 9901)*. Springer, 424–432. [doi:10.1007/978-3-319-46723-8_49](https://doi.org/10.1007/978-3-319-46723-8_49)

[26] Olaf Ronneberger, Philipp Fischer, and Thomas Brox. 2015. U-Net: Convolutional Networks for Biomedical Image Segmentation. In *Medical Image Computing and Computer-Assisted Intervention – MICCAI 2015 (LNCS, Vol. 9351)*. Springer, 234–241. [doi:10.1007/978-3-319-24574-4_28](https://doi.org/10.1007/978-3-319-24574-4_28)

[27] Saikat Roy et al. 2023. MedNeXt: Transformer-Driven Scaling of ConvNets for Medical Image Segmentation. In *Medical Image Computing and Computer Assisted Intervention – MICCAI 2023 (LNCS, Vol. 14223)*. Springer. [doi:10.1007/978-3-031-43901-8_39](https://doi.org/10.1007/978-3-031-43901-8_39)

[28] Jiacheng Ruan, Jincheng Li, and Suncheng Xiang. 2025. VM-UNet: Vision Mamba UNet for Medical Image Segmentation. *ACM Transactions on Multimedia Computing, Communications, and Applications* (2025). [doi:10.1145/3767748](https://doi.org/10.1145/3767748) Just Accepted.

[29] Jiacheng Ruan, Suncheng Xiang, Mingyu Xie, Ting Liu, and Yuzhuo Fu. 2022. MALUNet: A Multi-Attention and Light-weight UNet for Skin Lesion Segmentation. In *2022 IEEE International Conference on Bioinformatics and Biomedicine (BIBM)*. 1150–1156. [doi:10.1109/BIBM55620.2022.9995040](https://doi.org/10.1109/BIBM55620.2022.9995040)

[30] Ashish Vaswani, Noam Shazeer, Niki Parmar, Jakob Uszkoreit, Llion Jones, Aidan N. Gomez, Łukasz Kaiser, and Illia Polosukhin. 2017. Attention Is All You Need. In *Advances in Neural Information Processing Systems (NeurIPS)*, Vol. 30.

[31] Wenzuan Wang, Chen Chen, Meng Ding, Hong Yu, Sen Zha, and Jiangyun Li. 2021. TransBTS: Multimodal Brain Tumor Segmentation Using Transformer. In *Medical Image Computing and Computer Assisted Intervention – MICCAI 2021*. Springer, 109–119. [doi:10.1007/978-3-030-87193-2_11](https://doi.org/10.1007/978-3-030-87193-2_11)

[32] Weijia Wang and Bill Lin. 2022. Optimizing 3D U-Net-based Brain Tumor Segmentation with Integer-arithmetic Deep Learning Accelerators. *ACM Journal on Emerging Technologies in Computing Systems* 18, 2 (2022). [doi:10.1145/3495210](https://doi.org/10.1145/3495210)

[33] Xiaosheng Wu, Qingyi Hou, Zhaozhao Xu, Chaosheng Tang, Shuihua Wang, Junding Sun, and Yudong Zhang. 2025. FCFdiff-Net: Full-conditional feature diffusion embedded network for 3D brain tumor segmentation. *Quantitative Imaging in Medicine and Surgery* 15, 5 (2025). [doi:10.21037/qims-](https://doi.org/10.21037/qims-)

24-2300

- [34] Hong-Yu Zhou, Jiansen Guo, Yinghao Zhang, Xiaoguang Han, Lequan Yu, Liansheng Wang, and Yizhou Yu. 2023. nnFormer: Volumetric Medical Image Segmentation via a 3D Transformer. *IEEE Transactions on Image Processing* 32 (2023), 4036–4045. [doi:10.1109/TIP.2023.3293771](https://doi.org/10.1109/TIP.2023.3293771)
- [35] Zongwei Zhou, Md Mahfuzur Rahman Siddiquee, Nima Tajbakhsh, and Jianming Liang. 2018. UNet++: A Nested U-Net Architecture for Medical Image Segmentation. In *Deep Learning in Medical Image Analysis and Multimodal Learning for Clinical Decision Support*. Springer, 3–11. [doi:10.1007/978-3-030-00889-5_1](https://doi.org/10.1007/978-3-030-00889-5_1)